

# Threading the Needle: Generating Textures in Nematics

Bryan Gin-ge Chen,<sup>1,2</sup> Paul J. Ackerman,<sup>3</sup> Gareth P. Alexander,<sup>4</sup> Randall D. Kamien,<sup>2</sup> and Ivan I. Smalyukh<sup>3</sup>

<sup>1</sup>*Instituut-Lorentz, Universiteit Leiden, Postbus 9506, 2300 RA Leiden, The Netherlands*

<sup>2</sup>*Department of Physics & Astronomy, University of Pennsylvania, Philadelphia PA 19104, USA*

<sup>3</sup>*Department of Physics, University of Colorado, Boulder, CO 80309, USA*

<sup>4</sup>*Department of Physics and Centre for Complexity Science,  
University of Warwick, Coventry, CV4 7AL, UK*

(Dated: November 4, 2018)

The Hopf fibration is an example of a texture: a topologically stable, smooth, global configuration of a field. Here we demonstrate the controlled sculpting of the Hopf fibration in nematic liquid crystals through the control of point defects. We demonstrate how these are related to torons by use of a topological visualization technique derived from the Pontryagin-Thom construction.

PACS numbers: 61.30.Jf, 61.30.Dk, 11.10.Lm

The combination of geometric order, optical response, and soft elasticity of liquid crystals uniquely positions them as an arena to study topology: boundary conditions on sample walls can obstruct smooth solutions in the bulk, forcing points, lines, and walls of diminished order [1]. In general, these topological defects serve as tools for probing the symmetries of the ground state manifold (GSM) [2], as fundamental excitations [3], and as potential building blocks for self-assembly [4]. Does topology only play a role in systems with *singularities*? Certainly not, the Skyrmion in two and three dimensions is an everywhere smooth complexion of order that is, nonetheless, topologically protected [5, 6]. Similar non-singular configurations are the origin, for instance, of gapless excitations in the quantum hall effect and topological insulators [7, 8]. In the case of nematic liquid crystals, the GSM is  $\mathbb{R}P^2$  and two- and three- dimensional Skyrmions are labelled by elements of the second and third homotopy groups,  $\pi_2(\mathbb{R}P^2)$  and  $\pi_3(\mathbb{R}P^2)$ , respectively. The non-trivial elements of the latter correspond to the much-storied “Hopf fibration” [9], an allowed texture in the nematic phase [10, 11]. In this Letter, we demonstrate our ability to controllably generate and robustly visualize the Hopf fibration in cholesteric systems: nematics with a preferential handedness, or twist.

Our starting point is the toron configuration depicted in Fig. 1 and described in detail in [12]. This is a tube of double-twist that is wrapped upon itself, its boundary forming a torus. Above and below the “donut hole,” there are two point defects, both taking the form of hyperbolic hedgehogs. By manipulating these two point defects we can create a defect free texture with the topology of the Hopf fibration as in Fig. 2. Recall that the preimage of an element of the GSM,  $\hat{\mathbf{n}}_0 \in \mathbb{R}P^2$ , is the set of points in the sample where the director field  $\hat{\mathbf{n}} = \hat{\mathbf{n}}_0$ . Because we are considering three-dimensional nematics, we have a map from a three dimensional space (the sample) to the two-dimensional GSM: it follows that the preimage of  $\hat{\mathbf{n}}_0$  is a closed curve with topology of one or more disjoint circles. The Hopf fibration is characterized by the

linking of the preimages of any two directions  $\hat{\mathbf{n}}_1 \neq \hat{\mathbf{n}}_2$ .

How do we know it is the Hopf fibration, and how does the topology work out to render this result? To answer the first question, we utilize the Pontryagin-Thom construction for visualization of nematic configurations [13, 14] which we now briefly sketch. This method is a three-dimensional generalization of the use of crossed polarizers to study Schlieren textures in two-dimensional samples with the director taking values in  $\mathbb{R}P^1$  [15].

Recall that the dark lines in a Schlieren texture mark those regions where the director is along one of the two polarizer directions; continuity ensures that the dark lines only end on point defects and topology ensures that an even number of dark lines emanate from each point defect. We can abstract this slightly by considering only half the lines, *i.e.*, those corresponding to just one of the polarizer directions; note that in either case, each line carries an arbitrarily chosen yet *globally* consistent orientation so that the lines point, say, from positive to negative defects.

This two-dimensional construction has a natural generalization to three dimensions. We first pick a probe direction  $\hat{\mathbf{p}} \in \mathbb{R}P^2$ . Next we draw the surface,  $\Sigma_{\hat{\mathbf{p}}} \in \mathbb{R}^3$ , on which the director is everywhere *perpendicular* to the probe,  $\hat{\mathbf{p}} \cdot \hat{\mathbf{n}} = 0$ . We are therefore looking at the preimage of a whole curve  $\hat{\mathbf{p}}_{\perp}$  in  $\mathbb{R}P^2$ , the “equator” if  $\hat{\mathbf{p}}$  were the “North pole.” Were we to look for the preimage of  $\hat{\mathbf{p}}$  we would generically only get a curve and, more problematically, we could get the empty set for a nontrivial texture. The surface construction, however, neatly generalizes the two-dimensional case: the boundaries of any surface must be topological defects. A line boundary is the location of a disclination line, carrying the  $\mathbb{Z}_2$  charge associated with  $\pi_1(\mathbb{R}P^2)$ , while a point boundary, *i.e.* a hole in the surface, carries a  $\mathbb{Z}$  charge associated with  $\pi_2(\mathbb{R}P^2)$  where here and throughout we only use based homotopy groups. The surfaces, however, do not carry enough information to determine the point charges. In order to capture this information, we must add an additional piece of information to the surface, namely the

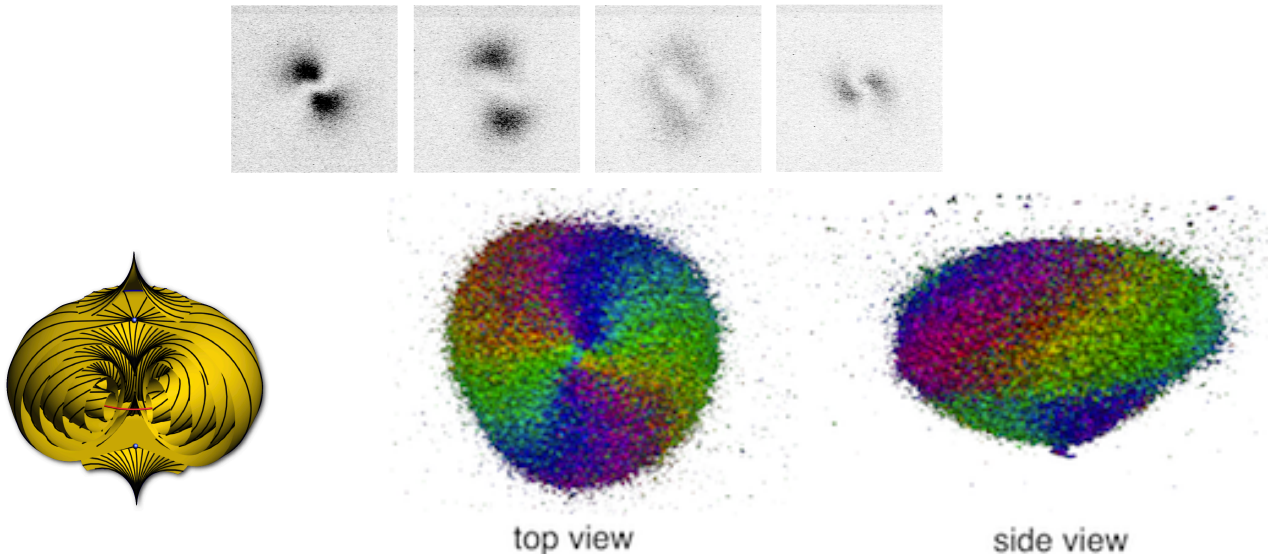


FIG. 1: The top figures shows selected 3PEF-PM images from an image stack – the images are  $16 \mu\text{m}$  wide and approximately  $4 \mu\text{m}$  apart in the  $z$ -direction. Bottom Left: the toron texture from [12]. Bottom Center and Right: the “Pontryagin-Thom” surface constructed from this image stack. The spots of color are an artifact of our construction scheme – they are places where the software has chosen the wrong branch. Fortunately, the robustness of this method allows us to recognize the overall texture. Note the two hedgehog defects on top and bottom.

direction of the director in  $\Sigma_{\hat{\mathbf{p}}}$ . We represent this pictorially through a color wheel, ranging from red to violet through orange, yellow, green, blue, and indigo. as the director rotates by  $\pi$ . We pass through the color wheel a second time if the director rotates by  $2\pi$ , as it does, for instance, in  $\Sigma_{\hat{\mathbf{z}}}$  for the standard radial hedgehog shown in Fig. 3. In fact, since all point defects in a uniaxial nematic can be oriented [23], the usual  $\hat{\mathbf{n}} \rightarrow -\hat{\mathbf{n}}$  symmetry does not come into play so the director will always rotate through the color wheel an even number of times, that is, rotations by multiples of  $2\pi$ . As a result, a point defect of charge  $p \in \pi_2(\mathbb{R}P^2)$  will have a winding of  $2p\pi$ , or will cover the color wheel  $2p$  times, providing a unique identification of point defects in nematics.

There is an important constraint on the colors that may paint the preimage. The neighborhood of the preimage  $\Sigma_{\hat{\mathbf{p}}}$  must admit a continuous map to the GSM [13] and the neighborhood of  $\hat{\mathbf{p}}_{\perp} \in \mathbb{R}P^2$  is a Möbius strip  $M$ , a line bundle over the equatorial circle. This means that the normal vectors to points in  $\Sigma_{\hat{\mathbf{p}}}$  are mapped continuously to points of  $M$  lying “above” the points of the base circle. Since one turn through the color wheel is half a trip through  $M$ , the surface normal on any path in  $\Sigma_{\hat{\mathbf{p}}}$  whose image in  $\mathbb{R}P^2$  wraps the equator once will reverse sign this extra structure forces every closed curve on  $\Sigma_{\hat{\mathbf{p}}}$  to have an even color winding so that the image of the surface normal in  $M$  can be continuous.

Finally, it can be shown that this representation is faithful, that is, up to homotopy, no information is lost and the original texture can be constructed from the representation we present here [14]. A further advantage is

that complicated homotopies of three-dimensional configurations can be visualized by manipulating the surfaces; not only continuous deformations but also a general class of merging of surfaces called bordisms.

In the experiments, we used nematic LC ZLI 2806 doped with the chiral agent CB15 to obtain the cholesteric pitch  $P$  of interest according to the relationship concentration of CB15  $C = 1/(h * P)$ , where  $h = 5.9 \mu\text{m}^{-1}$  is the helical twisting power of the used combination of the nematic host and chiral additive. Our cholesteric mixture had  $P = 20 \mu\text{m}$  to match the thickness of the used capillary  $d$  so that  $d/P = 1$ . A rectangular capillary with  $20 \times 200 \mu\text{m}$  cross-section was treated for vertical surface boundary conditions by infiltrating it with a 0.1wt.% aqueous solution of a surfactant [3-(trimethoxysilyl)propyl]octadecyldimethylammonium chloride (DMOAP) and then evaporating the solution by heating it to  $90^\circ\text{C}$  and keeping it at this temperature for about 30 min. The cholesteric mixture was then heated to isotropic phase at  $80^\circ\text{C}$  and infiltrated to the capillary to avoid filling-induced defects. Various twist-stabilized localized structures in an initially unwound frustrated cholesteric LC were formed through the use of holographic optical tweezers (HOT) [16] built around a spatial light modulator (SLM) and a CW laser operating at  $1064\text{nm}$ . Laser beams of power less than  $50\text{mW}$  were focused and spatially steered in 3D within the sample. We have used 10X-100X microscope objectives with numerical apertures ranging within  $\text{NA}=0.1-1.4$  for optical generation.

Imaging of the samples utilized three-photon excitation

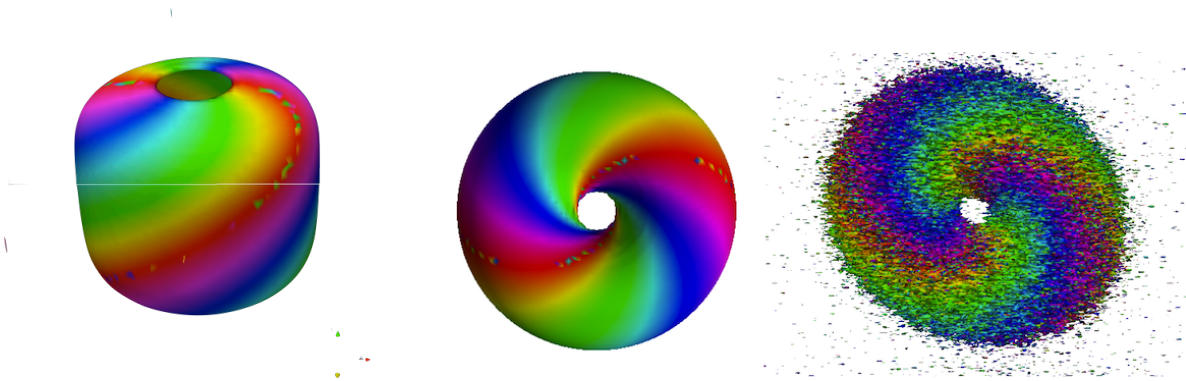


FIG. 2: On the left we show a simulation texture of a toron in which the point hedgehogs are replaced with disclination loops. Bringing those loops together through the center of the spool gives a torus with linked preimages. In the center, we show a simulation of the resulting Hopf fibration. On the right, we show an experimental image of the same texture.

fluorescence polarizing microscopy (3PEF-PM) [17] integrated with HOT into a single optical setup built around the same inverted optical microscope IX-81 (Olympus). The optical technique of 3PEF-PM [17] is non-invasive, does not require dyes (since the detected fluorescence comes from the LC molecules themselves), and enables the imaging of director fields in 3D. The non-linear three-photon absorption process gives rise to a  $\cos^6 \beta$  orientational dependence of the fluorescence signal, where  $\beta$  is the angle between the probing light's linear polarization and the director. The inherent  $z$ -resolution (along the microscope's optical axis) associated with the non-linear process allows for optical sectioning and reconstruction of 3D images of the director field. 3D 3PEF-PM images for four linear polarizations are used to generate a representation in Paraview [20].

Whereas Schlieren textures in thin cells give directly the Pontryagin-Thom construction for (quasi)-two-dimensional nematics, the analogous colored surfaces of three-dimensional textures are not an automatic output of any current imaging technique. These surfaces can be extracted easily from knowledge of the director field, which can in turn be obtained from confocal microscopy [18, 19] or polarizing-mode nonlinear optical microscopies such as 3PEF-PM, coherent anti-Stokes Raman scattering microscopy [21], and stimulated Raman scattering microscopy [22]. To construct this surface, we take intensity data from confocal slices, polarized at four different angles  $\pi/4$  apart in the  $xy$  plane ( $E_0^2, E_{\pi/4}^2, E_{\pi/2}^2, E_{3\pi/4}^2$ ). The Stokes parameters  $I, Q$ , and  $U$  are:

$$I = \frac{1}{2} \left( E_0^2 + E_{\pi/4}^2 + E_{\pi/2}^2 + E_{3\pi/4}^2 \right), \quad (1)$$

$$Q = E_0^2 - E_{\pi/2}^2, \quad (2)$$

$$U = E_{\pi/4}^2 - E_{3\pi/4}^2. \quad (3)$$

Writing  $\hat{\mathbf{n}} = [\sin \theta \cos \phi, \sin \theta \sin \phi, \cos \theta]^T$  and taking the electric field amplitude to simply be proportional to the

local electric anisotropy tensor we find that  $I \propto J \sin^n \theta$  and  $Q/U = \tan(2\phi)$  where  $J$  is the amplitude of the signal. Here  $n$  is an exponent depending on the imaging modality;  $n = 4$  for the case of fluorescence confocal microscopy [18, 19],  $n = 6$  for 3PEF-PM with fluorescence detection without a polarizer [17], and  $n = 8$  for coherent anti-Stokes Raman scattering polarizing microscopy with linearly polarized detection collinear with the polarization of excitation light. Away from the toron the director is normal to the top and bottom surface and so  $\theta = 0$  there. Thus we may shift and normalize the calculated  $I$  from the data to take values from 0 to 1 so that the  $n$ th root of  $I$  gives us  $\sin \theta$ . The angle  $\phi$  then gives us the angle of the polarization projected to the  $xy$  plane, and we can reconstruct the director  $\hat{\mathbf{n}}$  from  $\theta$  and  $\phi$ .

To go from this to the colored surface numerically, we reflect the director field so that it lies in the upper half of the sphere, *i.e.* if  $\cos \theta < 0$  we take  $\hat{\mathbf{n}} \rightarrow -\hat{\mathbf{n}}$ . Using Paraview [20] we then view the isocontour with  $n_z$  close to zero. Though one might want to take a slice with  $n_z$  zero, the non-orientability of the line field makes it difficult to exclude the artificial “branch cuts” where any reconstruction assigns adjacent grid points to different branches of  $\hat{\mathbf{n}}$ , for example when  $\hat{\mathbf{n}}$  happens to be adjacent to a data point of  $-\hat{\mathbf{n}}$ . The downside of our approach is that what should be one surface at  $n_z = 0$  is actually two nearby surfaces  $n_z = \pm \epsilon$ . Note that all we pick out here are the surfaces of (near) maximum  $I$ , so the sixth-root transformation we made above actually makes no difference; all we need is the fact that the regions in the data where  $I$  is maximum correspond to regions where the molecules tend to lie in the  $xy$  plane.

We analyzed 3PEF-PM images of several chirally doped nematic textures as described. A precise reconstruction of the director field requires a careful analysis of the optical properties of the material. However, this is unnecessary to determine topological features, which are independent of the fine details and depend only on the coarse structure that is preserved under continuous defor-



FIG. 3: On the left we show a schematic of a hedgehog/anti-hedgehog pair. They are of opposite sign because the sense of their color rotations is of opposite handedness. Note, however, that viewed from below the handedness of each color wheel changes, illustrating the global sign ambiguity. On the right we show a schematic of the same pair of defects moved one on top of each other with the surface bent around. Were we to neglect the orientation imposed by the surface normal, we might think the two defects are of the same sign. The surface keeps track of the global base point.

mation. Thus even a highly approximate reconstruction of the director will capture all of the topology correctly.

Using these tools, we show the toron texture in this Pontryagin-Thom representation in Fig. 1, alongside the director picture [12]. The colored stripes on the squashed sphere depict the double-twist inside the torus. On top and bottom the color twists around signaling a hedgehog/anti-hedgehog pair. The surface has no boundary and thus there are no disclination lines. It follows that we can globally orient the texture (up to an overall sign choice) to make it a vector on  $S^2$ . Thus, by construction, the surface separates space into an outer region where the director lifts to a vector in the northern hemisphere  $n_z > 0$  and an inner region where it maps to the southern hemisphere  $n_z < 0$ . This immediately tells us that there is *not* a Hopf fibration: recall that to measure the degree of the Hopf fibration one takes the preimage of two directions on  $S^2$ , each a closed loop, and calculates the linking number of the two preimages. The linking number is independent of which two preimages we take and so, if we take a loop where the vector field is in the southern hemisphere it *can not* link with a preimage of a vector in the northern hemisphere – the two loops are separated from each other by the surface in Fig. 1! To create a non-zero linking number, we must somehow entangle the preimages. Fortunately, the nematic symmetry allows us to easily visualize this.

In nematics, disclination loops can carry hedgehog charge [23]. As seen in experiment [12] the two point defects in Fig. 1 can both open up into disclination loops. Now there is a passageway between the inside and the outside of the Pontryagin-Thom surface and we can no longer orient the director field. Nonetheless, we can now bring the two loops together through the eye of the spool shown on the left in Fig. 2. Once brought together they cancel and we again have a situation with no disclinations. Again, we can orient the director field and the torus separates the northern and southern hemispheres. We now see in both the simulated textures and, more importantly, in the experiment that the constant colored circles on the torus link with each other – the preim-

ages of different directions are linked! We have created a degree-one Hopf fibration starting from the toron.

In closing, we note that this graphical representation immediately makes clear a number of often subtle issues in the description of defects in nematics [23]. First, we can see how the relative charges of two defects depends upon a base point: in this representation, a positive point defect will have a counter-clockwise-rotating color wheel, while a negative point defect will have a clockwise-rotating color wheel when we look from above. Were we to look at the same surface from below, however, the handedness of the rotations flip! This corresponds to the global ambiguity in choosing charge associated with the two choices of lifting  $\mathbb{R}P^2$  to  $S^2$ . It follows that looking at two pieces of surface in the vicinity of two defects does not allow the calculation of their relative degree – one surface must be used in order to consistently determine the topological charge. Finally note that these surfaces can end on disclination lines, just as the dark brushes in the Schlieren texture can end on disclination points in two-dimensions. Importantly, the construction of a colored surface from any given liquid crystal texture captures all of the topological information about the texture, and also permits the full director field to be reconstructed, at least up to homotopy. In future work we will use this method to visualize blue phases and other complex textures. Generalizing to biaxial nematics is another extension worth pursuing.

We acknowledge stimulating discussions with D. Beller, F. Cohen, and R. Kusner. GPA, BGC, and RDK were supported in part by NSF DMR05-47230 and a gift from L.J. Bernstein. This research was supported in part by the National Science Foundation under Grant No. NSF PHY11-25915. GPA, BGC, RDK, and IIS thank the KITP for their hospitality while this work was being prepared. BGC thanks the hospitality of the Boulder School in Condensed Matter and Materials Physics where some of this work was completed.

- 
- [1] M. Kléman, *Points, Lines, and Walls*, (John Wiley & Sons, New York, 1983).
- [2] N.D. Mermin, *Rev. Mod. Phys.* **51**, 591 (1979).
- [3] J.M. Kosterlitz, D. J. Thouless, 1973, *J. Phys. C: Solid State Phys.*, **6**, 1181 (1973).
- [4] D.R. Nelson, *Nano Lett.*, **2** (10), 1125 (2002).
- [5] T.H.R. Skyrme, *Nucl. Phys.* **31**, 556 (1962).
- [6] N.S. Manton and P.M. Sutcliffe, *Topological Solitons*, (Cambridge University Press, Cambridge, 2004).
- [7] D.J. Thouless, M. Kohmoto, M.P. Nightingale, and M. den Nijs, *Phys. Rev. Lett.* **49**, 405 (1982).
- [8] C.L. Kane and E.J. Mele, *Phys. Rev. Lett.* **95**, 146802 (2005).
- [9] H. Hopf, *Math. Ann.* **104**, 637 (1931).
- [10] Y. Bouligand, *J. Phys. France* **35**, 959 (1974).
- [11] Y. Bouligand, B. Derrida, V. Poénaru, Y. Pomeau, and G. Toulouse, *J. Phys. France* **39**, 863 (1978).
- [12] I.I. Smalyukh, Y. Lansac, N.A. Clark, and R. Trivedi, *Nat. Mater.* **9**, 139 (2010).
- [13] B.G. Chen, *Topological Defects in Nematics and Smectic Liquid Crystals*, University of Pennsylvania Ph.D. Thesis (2012).
- [14] T. tom Dieck, Chapter 13, *Algebraic Topology*, Eur. Math. Soc. (2008).
- [15] A variant of this has been used, for instance, to visualize the braiding of Majorana modes in three dimensional topological insulator–superconductor systems. See J.C.Y. Teo, C.L. Kane, *Phys. Rev. Lett.* **104**, 046401 (2010).
- [16] R. T. Trivedi, T. Lee, K. A. Bertness, and I. I. Smalyukh, *Optics Express* **18**, 27658 (2010).
- [17] T. Lee, R.P. Trivedi, and I.I. Smalyukh, *Opt. Lett.* **35**, 3447 (2010).
- [18] I.I. Smalyukh, S.V. Shiyakovskii, and O.D. Lavrentovich, *Chem. Phys. Lett.* **336**, 88 (2001).
- [19] I.I. Smalyukh and O.D. Lavrentovich, *Phys. Rev. E* **66**, 051703 (2002).
- [20] A.H. Squillacote, *The ParaView Guide: A Parallel Visualization Application* (Kitware, Inc., 3<sup>rd</sup> edition, 2008) Software available at <http://paraview.org>.
- [21] A. Kachynskii, A. Kuzmin, P.N. Prasad, and I.I. Smalyukh, *Appl. Phys. Lett.* **91**, 151905 (2007).
- [22] T. Lee, B. Senyuk, R.P. Trivedi, and I.I. Smalyukh, *Optical microscopy of soft matter systems*. In press. In *Soft Matter*, A. Fernandez De Las Nieves (ed.), Wiley-VCH, (2013).
- [23] G.P. Alexander, B.G. Chen, E.A. Matsumoto, and R.D. Kamien, *Rev. Mod. Phys.* **84**, 497 (2012).